

MULTI-EPOCH LOW RADIO FREQUENCY SURVEYS OF THE *KEPLER K2* MISSION CAMPAIGN FIELDS  
3, 4, AND 5 WITH THE MURCHISON WIDEFIELD ARRAY

TINGAY, S.J.<sup>1</sup> AND HANCOCK, P.J.<sup>1</sup>

<sup>1</sup>*International Centre for Radio Astronomy Research, Curtin University, Bentley, WA 6102, Australia*

ABSTRACT

We present Murchison Widefield Array (MWA) monitoring of the Kepler K2 mission Fields 3, 4, and 5 at frequencies of 155 and 186 MHz, from observations contemporaneous with the K2 observations. This work follows from previous MWA and GMRT surveys of Field 1, with the current work benefiting from a range of improvements in the data processing and analysis. We continue to build a body of systematic low frequency blind surveys overlapping with transient/variable survey fields at other wavelengths, providing multi-wavelength data for object classes such as flare stars. From the current work, we detect no variable objects at a surface density above  $2 \times 10^{-4}$  per square degree, at flux densities of  $\sim 500$  mJy, and observation cadence of days to weeks, representing almost an order of magnitude decrease in measured upper limits compared to previous results in this part of observational parameter space. This continues to show that radio transients at metre and centimetre wavelengths are rare.

*Keywords:* catalogs; galaxies: active; instrumentation: interferometers; radio continuum: general

## 1. INTRODUCTION

The Kepler K2 mission commenced in 2014, designed to use the Kepler spacecraft with a reduced number of reaction wheels, to observe a number of fields near the ecliptic (Howell et al. 2014).

Previously, we undertook a pilot study of the K2 Field 1 using the Murchison Widefield Array (MWA: Tingay et al. (2013)) and the TGSS ADR1 (Intema et al. 2017) using the Giant Metre-wave Radio Telescope (GMRT: Swarup (1991)) to monitor the field at low frequencies (140 - 200 MHz) during the K2 campaign (Tingay et al. 2016). We produced a source catalog for this field containing over 1000 radio sources. No transient or variable radio sources were found during the Field 1 MWA campaign; the catalog produced a unique supporting resource for K2 mission science.

Using the lessons learned during the Field 1 MWA observations and subsequent data processing, we have now undertaken further monitoring observations of K2 Fields 3, 4, and 5 concurrent with the K2 observations. We report these observations in this paper. We used an improved scheduling strategy for these new observations, allowing a more robust and accurate extraction of radio light curves from our data. Thus, our sensitivity to transients and variables is improved, relative to the results reported in Tingay et al. (2016).

The K2 mission is making significant strides in the direction blazed by Kepler, in the detection and study of large numbers of exoplanets. However, the science goals of K2 observations are widely varied. Of relevance to the results of our MWA monitoring of K2 fields, a range of work aimed at studying the optical variability of active galactic nuclei (AGN) is starting to emerge (Smith et al. 2017; Wehrle et al. 2018; Carini et al. 2017). K2 has also detected M dwarf flare stars that require study at radio frequencies, in particular low frequencies where such stars are most active (Villadsen et al. 2018).

A search for M dwarf flares was performed with our previously published data for K2 Field 1, adding to a growing literature in this field that is relevant to exoplanet habitability research. In particular, our previous K2 Field 1 results and the MWA results of Rowlinson et al. (2016) did not detect any M dwarf flares. However, using the MWA to measure circular polarisation and therefore achieve higher sensitivity to flares, Lynch et al. (2017) found intermittent flares from targeted observations of UV Ceti, but not from YZ CMi or CN Leo. Only sparse observational data exist at MWA frequencies for M dwarf flare stars and further systematic monitoring studies are required, as well summarised in §5.3.3 of the review by Matthews (2019). The TESS mission (Ricker et al. 2015) is being used to monitor large numbers of M dwarf flares (Günther et al. 2019) during the Cycle 1 portion of the mission, covering southern declinations well matched to follow-up with MWA observations.

While various classes of radio transients are expected to be rare at centimeter and meter wavelengths (Metzger et al. 2015), significant work is being expended testing these limits (Bell et al. 2014; Carbone et al. 2016; Croft et al. 2013; Murphy et al. 2015; Obenberger et al. 2015; Polisensky et al. 2016; Rowlinson et al. 2016; Murphy et al. 2017) with existing large-scale instruments and detecting occasional interesting transients and variables (Hyman et al. 2005, 2009; Jaeger et al. 2012; Murphy et al. 2017). Much of this work is in preparation for transient research with the Square Kilometre Array (SKA, Fender et al. 2015).

Often through radio transient surveys, once detections are made, the follow-up identification, verification, and interpretation of the objects is difficult. The goal of the observations reported here is to continue to build unbiased, wide-field, multi-epoch surveys at low radio frequencies, covering the full extent of the K2 fields concurrent with the optical monitoring observations, to facilitate the multi-wavelength search for transients and variables. In §2 we present the observations and data processing, including improvements over Tingay et al. (2016). In §3 we present our results, and we discuss them and our conclusions in §4.

## 2. OBSERVATIONS AND DATA PROCESSING

### 2.1. Observations

The parameters of the MWA observations conducted for K2 fields 3, 4, and 5 are given in Table 1, for the period 2014 November 07 to 2015 May 28. All observations were performed in a standard imaging mode, as described in Tingay et al. (2016), at the same center frequencies of 154.88 MHz and 185.60 MHz and with the same processed bandwidth of 30.72 MHz ( $24 \times 1.28$  MHz coarse channels, each comprised of  $128 \times 10$  kHz fine channels).

However, the scheduling of these observations benefited from our prior experiences recorded in Tingay et al. (2016), in that we used a single az/el pointing for each of the three fields of interest. This guarantees that all observations for a given field have the same LST, and thus a primary beam and synthesized beam that are consistent throughout the observation sequence. This results in data that are simpler to process in terms of extracting light curves and more robust light curves due to smaller errors on individual flux densities.

We recovered the MWA data from the new MWA All-Sky Virtual Observatory (ASVO) node<sup>1</sup>, which allows users to discover observations and download the visibility and calibration data in a variety of formats, applying user-defined manipulations to the visibilities. We downloaded the observations described in Table 1 using an averaging time of 2 seconds, a frequency averaging of 40 kHz (corresponding to four fine channels), and flagging 160 kHz at the edges of coarse channels (corresponding to 16 fine channels at each coarse channel edge). Recorded flagging information was also applied, as was default radio frequency interference (RFI) flagging via AO Flagger (Offringa et al. 2012). The visibility data were extracted as uvfits files, suitable for import into MIRIAD (Sault et al. 1995).

The total volume of MWA visibility data processed (including calibration data) was approximately 4.4 TB, with the visibility averaging parameters described above applied during data extraction from the ASVO.

For Field 3, 36 observations were scheduled, but only 18 were successful. 18 observations between 2014 November 25 and 2014 December 13 were affected by a lightning strike that caused a power outage at the MWA (completely lost four observations) and caused temporary damage to 43/128 tiles (substantially degraded data). Thus, only the 18 successful observations are listed in Table 1 and described in the remainder of the paper.

Other issues with data from other Fields are described in the following section, primarily regarding challenges introduced by the far northern pointings and strong sources in the high response primary beam sidelobes. Any future monitoring of K2 fields with the MWA could concentrate on fields south of the equator, to minimise such issues.

**Table 1.** MWA observation log

OBSID	START DATE/TIME (UT)	T (s)	TARGET	FREQ (MHz)	RA (°)	DEC (°)
1099403792	2014-11-07 13:56:16	296	F3	154.88	334.454	-14.675
1099392080	2014-11-07 10:41:03	176	3C444	154.88	330.524	-19.773
1099404096	2014-11-07 14:01:19	296	F3	185.60	335.724	-14.676
1099392256	2014-11-07 10:43:59	176	3C444	185.60	331.26	-19.774
1099576120	2014-11-09 13:48:24	296	F3	154.88	334.453	-14.675
1099478520	2014-11-08 10:41:43	176	3C444	154.88	331.678	-19.774
1099576424	2014-11-09 13:53:27	296	F3	185.60	335.723	-14.676
1099478704	2014-11-08 10:44:48	176	3C444	185.60	332.447	-19.775
1099748448	2014-11-11 13:40:32	296	F3	154.88	334.452	-14.675
1099910736	2014-11-13 10:45:19	176	3C444	154.88	330.274	-19.968
1099748752	2014-11-11 13:45:35	296	F3	185.60	335.723	-14.676
1099910920	2014-11-13 10:48:24	176	3C444	185.60	331.043	-19.968
1099920776	2014-11-13 13:32:40	296	F3	154.88	334.452	-14.675
1099910736	2014-11-13 10:45:19	176	3C444	154.88	330.274	-19.968
1099921080	2014-11-13 13:37:43	296	F3	185.60	335.722	-14.676
1099910920	2014-11-13 10:48:24	176	3C444	185.60	331.043	-19.968
1100093104	2014-11-15 13:24:48	296	F3	154.88	334.451	-14.675
1100083632	2014-11-15 10:46:55	176	3C444	154.88	332.647	-19.969
1100093408	2014-11-15 13:29:51	296	F3	185.60	335.722	-14.676
1100083808	2014-11-15 10:49:51	176	3C444	185.60	333.383	-19.969
1100265432	2014-11-17 13:16:56	296	F3	154.88	334.45	-14.675

*Table 1 continued on next page*

<sup>1</sup> <https://asvo.mwatelescope.org/>

Table 1 (continued)

1100256520	2014-11-17 10:48:24	176	3C444	154.88	334.987	-19.97
1100265736	2014-11-17 13:21:59	296	F3	185.60	335.721	-14.676
1100256704	2014-11-17 10:51:27	176	3C444	185.60	335.756	-19.971
1100437760	2014-11-19 13:09:04	296	F3	154.88	334.45	-14.675
1100429416	2014-11-19 10:50:00	176	3C444	154.88	330.124	-19.773
1100438064	2014-11-19 13:14:07	296	F3	185.60	335.72	-14.676
1100429592	2014-11-19 10:52:56	176	3C444	185.60	330.859	-19.773
1100610096	2014-11-21 13:01:20	296	F3	154.88	334.483	-14.675
1100602304	2014-11-21 10:51:27	176	3C444	154.88	332.464	-19.774
1100610392	2014-11-21 13:06:16	296	F3	185.60	335.72	-14.676
1100602488	2014-11-21 10:54:31	176	3C444	185.60	333.233	-19.775
1100782416	2014-11-23 12:53:19	296	F3	154.88	334.449	-14.675
1100775200	2014-11-23 10:53:04	176	3C444	154.88	334.837	-19.776
1100782720	2014-11-23 12:58:24	296	F3	185.60	335.719	-14.676
1100775376	2014-11-23 10:56:00	176	3C444	185.60	335.573	-19.776
1108551264	2015-02-21 10:54:08	296	F4	154.88	56.437	19.719
1108734680	2015-02-23 13:51:04	112	HydA	154.88	138.646	-11.143
1108551560	2015-02-21 10:59:03	296	F4	185.60	57.677	19.721
1108734808	2015-02-23 13:53:11	112	HydA	185.60	139.181	-11.143
1108725688	2015-02-23 11:21:12	296	F4	185.60	57.344	21.244
1108734808	2015-02-23 13:53:11	112	HydA	185.60	139.181	-11.143
1109070040	2015-02-27 11:00:23	296	F4	154.88	56.073	21.243
1108986336	2015-02-26 11:45:20	112	HydA	154.88	135.448	-11.788
1114081920	2015-04-26 11:11:43	296	F5	154.88	131.325	18.973
1114036848	2015-04-25 22:40:32	176	3C444	154.88	332.197	-18.177
1114082216	2015-04-26 11:16:39	296	F5	185.60	132.563	18.974
1114037024	2015-04-25 22:43:28	176	3C444	185.60	332.933	-18.177
1114254248	2015-04-28 11:03:52	296	F5	154.88	131.325	18.973
1114209712	2015-04-27 22:41:36	176	3C444	154.88	334.437	-18.178
1114254544	2015-04-28 11:08:47	296	F5	185.60	132.562	18.974
1114209888	2015-04-27 22:44:32	176	3C444	185.60	335.172	-18.179
1114598904	2015-05-02 10:48:08	296	F5	154.88	131.324	18.973
1114555432	2015-05-01 22:43:35	176	3C444	154.88	331.437	-19.186
1114599200	2015-05-02 10:53:04	296	F5	185.60	132.561	18.974
1114555616	2015-05-01 22:46:39	176	3C444	185.60	332.206	-19.187
1114943560	2015-05-06 10:32:24	296	F5	154.88	131.322	18.973
1114901160	2015-05-05 22:45:44	176	3C444	154.88	335.916	-19.189
1114943856	2015-05-06 10:37:20	296	F5	185.60	132.559	18.974
1114901344	2015-05-05 22:48:48	176	3C444	185.60	336.686	-19.19

Table 1 continued on next page

**Table 1** (*continued*)

1115632872	2015-05-14 10:00:56	296	F5	154.88	131.32	18.973
1115592624	2015-05-13 22:50:07	176	3C444	154.88	330.366	-19.971
1115805200	2015-05-16 09:53:04	296	F5	154.88	131.319	18.973
1115765488	2015-05-15 22:51:11	176	3C444	154.88	332.606	-19.972
1115805504	2015-05-16 09:58:07	296	F5	185.60	132.59	18.974
1115765664	2015-05-15 22:54:07	176	3C444	185.60	333.342	-19.973

NOTE—Column 1 - MWA observation ID; Column 2 - UT date and time of observation start; Column 3 - duration of observation in seconds; Column 4 - observation target (F3 = Field 3; F4 = Field 4; F5 = Field 5; HydA = Calibrator Hydra A; 3C 444 = Calibrator 3C444); Column 5 - Centre frequency in MHz; Column 6 - Right Ascension in decimal degrees; and Column 7 - Declination in decimal degrees. The full observation table is available as a Machine Readable Table (CSV format).

## 2.2. Data Processing

### 2.2.1. Calibration and Imaging

Data processing proceeded as described in Sections 3.1.1 and 3.1.2 in [Tingay et al. \(2016\)](#) and readers are referred to those descriptions for details. An additional calibrator was used for our processing for K2 fields 3, 4, and 5, 3C 444. In cases where 3C 444 is the calibrator, the model for the flux density was parameterized as  $79.6 \frac{\nu}{160\text{MHz}}^{-0.88}$  Jy and a restriction in self-calibration was applied when imaging the calibrator, such that only baselines in the uv range 0.05 to 0.8 k $\lambda$  were used against this model.

Fields 4 and 5 are at significant positive declinations,  $\sim +19^\circ$  and  $\sim +17^\circ$ , respectively, compared to Field 3 at  $\sim -11^\circ$ . Imaging and calibration proved less consistently of high quality for Fields 4 and 5 than for Field 3. While all three fields provided high quality images at some epochs (examples shown in Figure 1), it was noted that a significant fraction of epochs for Fields 4 and 5 produced unusable images with the procedure described in [Tingay et al. \(2016\)](#). In some of these cases, we were able to recover images of a quality to be usable by removing from our imaging and calibration pipeline the final self-calibration step that included amplitude self-calibration.

Possible reasons for Fields 4 and 5 being more challenging for imaging and calibration could be ionospheric activity through a greater path length at low elevations, radio frequency interference at lower elevation observations, or the presence of nearby bright radio sources in the primary beam sidelobes (e.g. the Crab Nebula, the Southern Galactic Plane, and the Sun, in various combinations), which have a high response for northern pointing directions. An inspection of the logs recording the instrument status at these epochs reveals no significant issues with the intrinsic data quality.

In some cases, the imaging and calibration process did not converge, after attempting a range of variations on the pipeline. In particular, no epoch for Field 4 in the month of 2015 March was recoverable. During those epochs, we noted that the far northern pointing produced sidelobes with a peak response of  $>0.5$  of the main beam, meaning comparable power was contained in the visibilities from the opposite side of the sky. In addition, the Sun was above the horizon at increasing elevations during the month. This combination makes reliable imaging and calibration extremely difficult and the data were discarded. The set of usable data are listed in Table 1.

### 2.2.2. Source Finding and Production of Light Curves

The images described in §2.2.1 were inspected manually to remove any which were not usable. The (effectively full-sky) images were then cropped to contain only a region of interest which was determined to be the largest region over which we could obtain accurate flux measurements. The usable area of Field 5 is less than that of Fields 3 and 4 due to the presence of the Galactic plane in one of the primary beam side-lobes which increased the image noise away from the beam center. The images were then processed using ROBBIE<sup>2</sup> - a work-flow for detecting and characterizing variable and transient events in radio astronomy images ([Hancock et al. 2018](#)). ROBBIE processes data in the following

<sup>2</sup> [www.github.com/PaulHancock/Robbie](http://www.github.com/PaulHancock/Robbie)

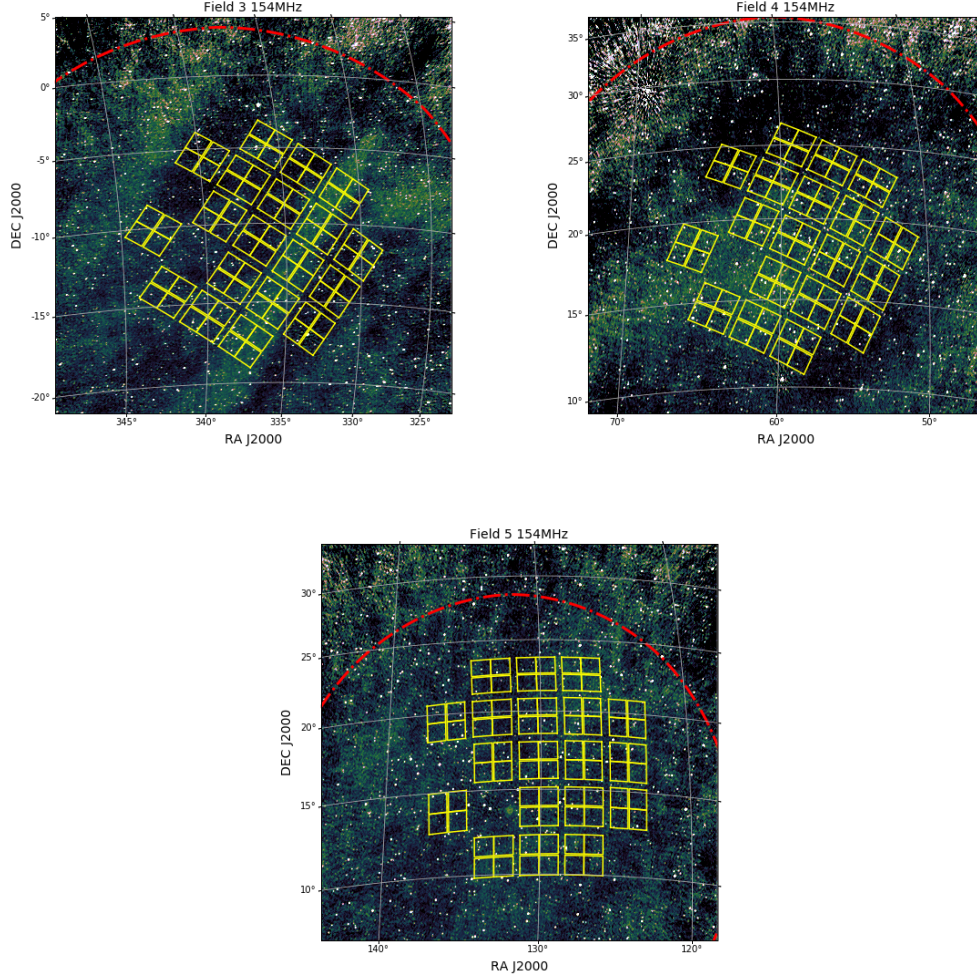


**Figure 1.** The three K2 fields monitored for variable and transient radio sources. Images shown are typical of those produced at the two frequencies, using the procedure described in the text, and have been cropped to show just the region covered by the Kepler sensors. The intensity scales range from  $-0.2$  to  $1$  Jy/beam. The K2 areal footprint is shown in a yellow overlay. The dot-dashed red circle shows the exclusion zone chosen by ROBBIE.

way. First, the individual epoch images are warped to remove any astrometric distortions introduced by the ionosphere, which are not captured in the calibration stage. This warping is done using FITS\_WARP<sup>3</sup> (Hurley-Walker & Hancock 2018). Next, the epochs are stacked to create an image cube, which is then flattened into a mean image. This mean image is then used to create a reference catalogue of persistent sources. For each of the persistent sources, ROBBIE creates a light curve using the so-called *priorized* fitting capability provided by AEGEAN<sup>4</sup> (Hancock et al. 2012, 2018). Each of the light curves are then characterized using standard metrics including the de-biased modulation index  $m_d$ ,  $\chi^2$ , and the false detection probability of seeing a given light curve variation given the uncertainties and a model of no variability. Each of the individual epoch images are then masked using the persistent source catalogue, and blind source finding is run on each to generate a list of candidate transient events. This list is then filtered for obvious false positives, and presented for further analysis.

We ran ROBBIE separately on each field/frequency combination making a total of six separate instances. Sources were identified as variable if their light curves had  $m_d > 0.05$  and false detection probability of  $p_{\text{val}} < 0.001$ . Four sources were identified as being variable in Field 5, with the variability being present at both frequencies. Closer

<sup>3</sup> [www.github.com/nhurleywalker/fits\\_warp](http://www.github.com/nhurleywalker/fits_warp)

<sup>4</sup> [www.github.com/PaulHancock/Aegean](http://www.github.com/PaulHancock/Aegean)

inspection of these light curves and images revealed that the cause of the variability was Jupiter moving through the field and passing close enough to persistent sources to become confused. This detection of Jupiter highlights the effectiveness of ROBBIE at detecting variability, but means that no astronomical (extra-solar system) variability was observed.

We inspected the list of candidate transient events and found that all the candidates were in one of four categories: sources that were below the  $5\sigma$  detection limit which were occasionally detected due to differing noise contributions, side-lobes of real sources that were not automatically excluded by ROBBIE, the Moon (present in a single epoch), or Jupiter when it was not being confused with persistent sources. We therefore find no astronomical transients in any of the six datasets.

### 3. RESULTS

As noted by Bell et al. (2011) and others, the density of transients and variables can be calculated from Poissonian statistics:

$$P(n) = \exp(-\rho\Omega) \quad (1)$$

where  $\rho$  is the surface density,  $\Omega$  is the sky area surveyed, and  $n$  is the number of variable or transient events. In the event of no detected events we can calculate the a 95% confidence upper limit on the surface density by setting  $P(n) = 0.05$  and solving for  $\rho$ . For multiple epochs and multiple pointing directions we can replace  $\Omega$  with the equivalent sky area:

$$\Omega_{eq} = \sum \Omega_i N_i \quad (2)$$

where  $\Omega_i$  and  $N_i$  are the sky coverage, and number of epochs for each pointing direction  $i$ . The number of epochs, sky area, and upper limit on the density of variable sources for each field are tabulated in Table 2. The variable source population probed by this work are those brighter than the detection limit in the mean image produced by ROBBIE. Since the sensitivity changes over the field of view we report the mean sensitivity for the variable sources in Table 2. The upper limit on the transient sources population, however, needs to consider the maximum image noise among all epochs. Thus we report a separate sensitivity for transient events in Table 2.

We combined data from all three fields to produce a combined detection limit. To do this, the effective area is equated as per Eq. 2, and we calculate the relevant sensitivity using:

$$\text{rms}_{Comb} = \frac{\sum \text{rms}_i N_i}{\sum N_i} \quad (3)$$

Field	$N_{epoch}$	Freq. (MHz)	Measured					Expected	
			$N_{src}$	$\Omega_i$ deg <sup>2</sup>	$\text{rms}^V$ (mJy)	$\text{rms}^T$ (mJy)	$\rho$ deg <sup>-2</sup>	$\bar{m}$ %	$\bar{\tau}_0$ year
3	9	154	2625	1028	88	230	$< 3.2 \times 10^{-4}$	16	2.9
3	9	185	2594	1028	65	380	$< 3.2 \times 10^{-4}$	17	1.9
4	2	154	1609	1028	225	1700	$< 1.5 \times 10^{-3}$	11	9.3
4	2	185	2168	1028	79	715	$< 1.5 \times 10^{-3}$	12	6.2
5	6	154	1814	718	78	192	$< 6.9 \times 10^{-4}$	12	5.1
5	5	185	1628	718	65	289	$< 8.3 \times 10^{-4}$	14	3.4

**Table 2.** Summary of data for the three fields of interest.  $N_{src}$  is the number of persistent sources detected.  $\Omega_i$  is the sky area used in Eq. 2. The sensitivity limit for variable sources ( $\text{rms}^V$ ) and transient sources ( $\text{rms}^T$ ) are separately reported as described in the text.  $\rho$  is a limit on the surface density of events detected in the survey as per Eq. 1, and is the same for variable and transient events since none were detected. The final two columns show the expected modulation index  $\bar{m}$  and characteristic timescale  $\bar{\tau}_0$  for refractive interstellar scintillation and are based on the SM2017 model.

In order to assess the implications of the data in Table 2, we must calculate the expected variability rate. The overwhelming majority of sources that are detected by the MWA are AGN. The characteristic timescale for AGN intrinsic variability is on the order of years to decades. Since the observations of the K2 fields were conducted on

time scales of days to weeks, we do not expect to see any intrinsic variability. Extrinsic variability, in the form of strong refractive interstellar scintillation (RISS), can be calculated using a model of scintillation based on Galactic  $H_\alpha$  intensity. Specifically, we use  $H_\alpha$  intensity from [Haffner et al. \(1998\)](#) as a proxy for scattering measure following their Eq 1. and Eq 16. of [Cordes & Lazio \(2002\)](#). This scattering measure is then used to calculate the diffractive scale using Eq 7a of [Macquart & Koay \(2013\)](#). These calculations are carried out using the SM2017<sup>5</sup> code, which assumes a scattering screen distance of 1 kpc. The modulation index and timescale of variability is calculated for each of the persistent sources in each of the fields at each frequency, and we report the mean of these in Table 2. The expected modulation indexes are 10 – 15%, which should be easily detectable given our selection criteria of  $m_d > 5\%$ . However the timescale of variability for RISS is 1 – 10 years, whereas our observations only cover timescales of days to weeks. The amount of variability seen on these shorter timescales would therefore be only  $\sim 1/300^{\text{th}}$  of the raw modulation index, below our ability to measure. The low expectation for variability, and the lack of observed variability are consistent corresponding to a low false detection rate for any transient sources found.

#### 4. DISCUSSION AND CONCLUSIONS

In Figure 2 we show the areal source density as a function of sensitivity for a selection of surveys at  $\sim 1$  GHz and 154 MHz. Also indicated is the minimum and maximum timescale that each survey is sensitive to.

In comparison to other radio surveys for variable and transient events (Figure 2), we find a significantly smaller surface density for each. Our upper limit on the density of variables is an order of magnitude lower than that found at comparable sensitivities by [Bannister et al. \(2011\)](#) and [Croft et al. \(2010\)](#) at higher frequencies ( $\sim 1$  GHz). We attribute this discrepancy to two effects: the difference in observing frequency; and the cadence of observations. The [Bannister et al. \(2011\)](#) and [Croft et al. \(2010\)](#) surveys were most sensitive to variability on the timescales of years to decades, whereas this work samples days to weeks. As predicted by the SM2017 model, we would expect RISS to have characteristic timescales of years to decades as per Table 2.

Also shown in Figure 2 are surveys at 154 MHz. [Bell et al. \(2014\)](#) used the MWA commissioning array to produce a survey with a  $5\sigma$  sensitivity of 5.5 Jy and a cadence of either less than 10 days or a year. They detect a single variable source giving a surface density of variables of  $1 \times 10^{-3} \text{ deg}^{-2}$  on year long time-scales, but find no variables on the shorter time-scales.

[Murphy et al. \(2017\)](#) compare the TIFR GMRT Sky Survey Alternative Data Release 1 (TGSS ADR1, [Intema et al. 2017](#)) and the GaLactic and Extragalactic All-sky Murchison Widefield Array (GLEAM, [Hurley-Walker et al. 2017](#)) survey catalogues and find a single variable source between two epochs separated by 1 – 3 years. However [Lynch et al. \(2017b\)](#) found no variable sources in their total intensity images created from nightly observations, and [Tingay et al. \(2016\)](#) found no variability in Kepler Field 1 on time-scales of days to a month. Shown in Figure 2, the combination of our Fields 3, 4, and 5 results provide the lowest upper limit ( $2 \times 10^{-4} \text{ deg}^{-2}$ ) at these frequencies, sensitivities (660 mJy), and cadences (day-month) from blind surveys.

[Carbone et al. \(2016\)](#) used 37 Dutch stations of LOFAR with a sub-set of the high band array, to survey four fields over a period of 6 months. They found no variable or transient sources, and their reported upper limit is shown as C16 in Figure 2. Additionally, [Carbone et al. \(2016\)](#) present a new method to represent the survey sensitivity for transient events as a function of the transient duration. In Figure 3 we replicate their results and add those for the Kepler fields F1, F3, and Comb, as described in Figure 2. The combined data set indicates a much lower limit on the rate of transients on timescales of 2 days ( $0.2 \text{ sky}^{-1} \text{ day}^{-1}$ ) to 1 month ( $0.06 \text{ sky}^{-1} \text{ day}^{-1}$ ). The upper limits for the transient rate of F1 and F3 in Figure 3, are nearly identical over the 2 – 16 day range. F1 has a smaller survey area than F3, but a greater number of epochs, and these two factors cancel out. The C16 survey has approximately 10 times the number of epochs as the F1/F3 surveys, but a field of view that is nearly  $1/70^{\text{th}}$  the size, resulting in a much less stringent upper limit. For transients of duration 2 – 16 days, the combined data of all three fields from this paper (Comb) has an effective field of view that is 3 times that of the individual surveys, and a similar distribution of epochs, resulting in a more stringent limit on the transient rate. In all, Figure 3 demonstrates the advantage of a wide field of view instrument such as the MWA with its ability to achieve high sensitivity to transient events in only a small number of observations.

Additional low frequency surveys are underway with the GMRT<sup>6</sup> and LOFAR ([Fender et al. 2006](#)), however they are yet to be published.

<sup>5</sup> [www.github.com/PaulHancock/SM2017/](http://www.github.com/PaulHancock/SM2017/)

<sup>6</sup> [www.tauceti.caltech.edu/stripe82/g1sts/](http://www.tauceti.caltech.edu/stripe82/g1sts/)



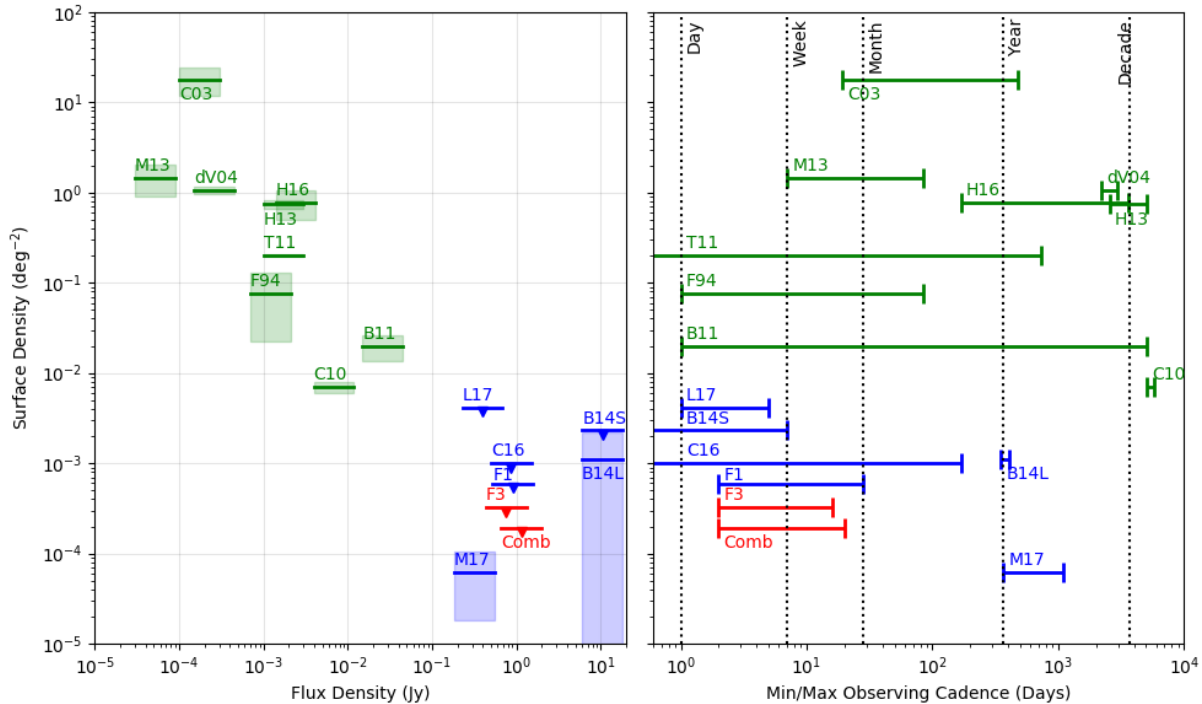


**Figure 2.** **Left:** Areal source density of variable sources as a function of survey sensitivity for surveys at  $\sim 1$  GHz (green), and  $\sim 150$  MHz (blue), as well as the current work at 154 MHz (red). Horizontal lines represent 1 – 3 times the detection limit, vertical shaded areas are uncertainties based on the number of detections, and triangles indicate upper limits. F3 is the upper limit from field 3 of this work at 154 MHz (the most sensitive individual limit), and Comb is the combination of fields 3 – 5 at the same frequency. **Right:** The min/max observing cadence for the same surveys, with colors as per the left panel. In this plot the surface density measurements and limits should vary as a function of time scale but that has not been taken into account. **References:** 1 GHz data: C03 Carilli et al. (2003), M13 Mooley et al. (2013), dV04 de Vries et al. (2004), H13 Hodge et al. (2013), H16 Hancock et al. (2016), T11 Thyagarajan et al. (2011), F94 Frail et al. (1994), B11 Bannister et al. (2011), C10 Croft et al. (2010). 150 MHz data: M17 Murphy et al. (2017), L17 stokes-I limits from Lynch et al. (2017b) on a daily cadence, C16 (Carbone et al. 2016), F1 Kepler field 1 from Tingay et al. (2016), B14S is the short duration limit and B14L is the long duration detection of variability from Bell et al. (2014).

The discrepancy between the detection and non-detections listed here can be explained by the different phase space that they are exploring: long versus short timescale variability. At 1 GHz variability is seen on timescales of days to decades, to varying degrees, whereas at 154 MHz the variability is only seen on year long time-scales. This difference is consistent with the  $H\alpha$  based modeling presented in the previous section, and means that at these frequencies intrinsic incoherent variability from AGN are on similar timescales to the extrinsic RISS induced variability, making the two difficult to disentangle. However, the corollary is that short time-scale variability must be dominated by other effects such as ionospheric and instrumental effects, but also intrinsic coherent emission. This makes the quiet incoherent low frequency sky an ideal place to look for coherent variability including: stellar flares (Lynch et al. 2017a); cyclotron maser emission from extra-solar planets (Farrell et al. 2004; Sirothia et al. 2014); prompt emission from gravitational wave events (Chu et al. 2016); fast radio bursts (Rowlinson et al. 2016; Tingay et al. 2015); and new classes of as-yet unidentified Galactic transients (Hyman et al. 2005; Jaeger et al. 2012). As such we anticipate that low-frequency surveys such as the GMRT 150 MHz Stripe 82 Transient Survey<sup>7</sup>, the LOFAR Transients Key Science Project (Fender et al. 2006), and MWA Transients Survey full data release (Bell et al. 2019), will be moving into a new area of discovery space that is more closely linked to the physics of the emission process rather than the physics of the interstellar medium. And in the more distant future, these surveys will be pathfinders for low frequency transient/variable surveys with the SKA.

<sup>7</sup> [www.tauceti.caltech.edu/stripe82/g1sts/](http://www.tauceti.caltech.edu/stripe82/g1sts/)

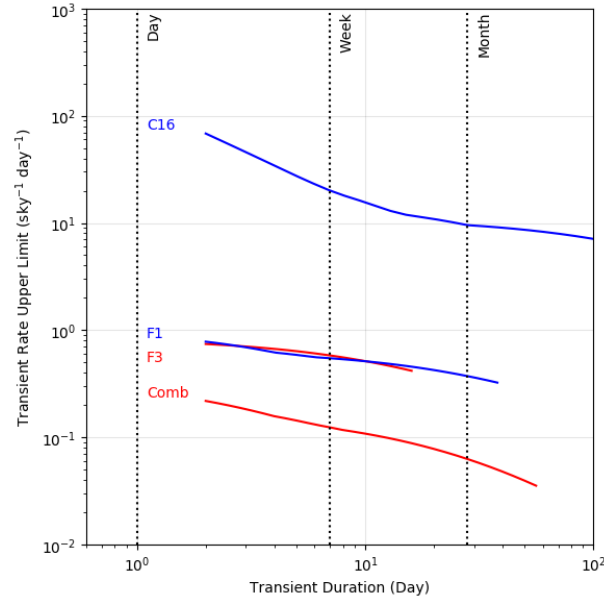


**Figure 3.** The transient rate upper limit for four of the surveys shown in Figure 2, for transients longer than 2 days. The upper limits take into account the distribution of observing epochs and the likelihood that a transient can occur between observations, as per the formalism of Carbone et al. (2016). The curves for F1 and F3 are nearly identical over 2 – 16 days.

## ACKNOWLEDGMENTS

### *SOFTWARE*

We acknowledge the work and support of the developers of the following software: Astropy (The Astropy Collaboration et al. (2013); Astropy Collaboration et al. (2018)), Numpy (van der Walt et al. 2011), Scipy (Jones et al. 2001), Pandas (McKinney 2010), AegeanTools (Hancock et al. 2018), Topcat (Taylor 2005), FITS\_WARP (Hurley-Walker & Hancock 2018), DS9<sup>8</sup>, ROBBIE (Hancock et al. 2018), and SM2017<sup>9</sup>.

This research made use of Astropy, a community-developed core Python package for Astronomy (The Astropy Collaboration et al. 2013; Astropy Collaboration et al. 2018).

### *FACILITIES*

This scientific work makes use of the Murchison Radio-astronomy Observatory, operated by CSIRO. We acknowledge the Wajarri Yamatji people as the traditional owners of the Observatory site. Support for the operation of the MWA is provided by the Australian Government (NCRIS), under a contract to Curtin University administered by Astronomy Australia Limited. We acknowledge the Pawsey Supercomputing Centre which is supported by the Western Australian and Australian Governments. This research has made use of NASA’s Astrophysics Data System.

*Facility:* Murchison Widefield Array

## REFERENCES

- Astropy Collaboration, Price-Whelan, A. M., Sipőcz, B. M.,  
et al. 2018, *The Astronomical Journal*, 156, 123
- Bannister, K. W., Murphy, T., Gaensler, B. M., Hunstead,  
R. W., & Chatterjee, S. 2011, *Monthly Notices of the  
Royal Astronomical Society*, 412, 634
- Bell, M. E., Fender, R. P., Swinbank, J., et al. 2011,  
*Monthly Notices of the Royal Astronomical Society*, 415,  
2
- Bell, M. E., Murphy, T., Kaplan, D. L., et al. 2014,  
*MNRAS*, 438, 352
- <sup>8</sup> ds9.si.edu  
<sup>9</sup> www.github.com/PaulHancock/SM2017/

- Bell, M. E., Murphy, T., Hancock, P. J., et al. 2019, *MNRAS*, 482, 2484
- Carbone, D., van der Horst, A. J., Wijers, R. A. M. J., et al. 2016, *MNRAS*, 459, 3161
- Carbone, D., van der Horst, A. J., Wijers, R. A. M. J., et al. 2016, *Monthly Notices of the Royal Astronomical Society*, 459, 3161
- Carilli, C. L., Ivison, R. J., & Frail, D. A. 2003, *The Astrophysical Journal*, 590, 192
- Carini, M. T., Brown, R., & Yik, H. 2017, in *American Astronomical Society Meeting Abstracts*, Vol. 229, *American Astronomical Society Meeting Abstracts #229*, 250.39
- Chu, Q., Howell, E. J., Rowlinson, A., et al. 2016, *Monthly Notices of the Royal Astronomical Society*, 459, 121
- Cordes, J. M., & Lazio, T. J. W. 2002, *ArXiv Astrophysics e-prints*, astro-ph/0207156
- Croft, S., Bower, G. C., & Whysong, D. 2013, *ApJ*, 762, 93
- Croft, S., Bower, G. C., Ackermann, R., et al. 2010, *The Astrophysical Journal*, 719, 45
- de Vries, W. H., Becker, R. H., White, R. L., & Helfand, D. J. 2004, *The Astrophysical Journal*, 127, 2565
- Farrell, W. M., Lazio, T. J. W., Zarka, P., et al. 2004, *Planetary and Space Science*, 52, 1469
- Fender, R., Stewart, A., Macquart, J. P., et al. 2015, *Advancing Astrophysics with the Square Kilometre Array (AASKA14)*, 51
- Fender, R. P., Wijers, R. A. M. J., Stappers, B., et al. 2006, in *VI Microquasar Workshop: Microquasars and Beyond*, eprint: arXiv:astro-ph/0611298, 104.1
- Frail, D. A., Kulkarni, S. R., Hurley, K. C., et al. 1994, *The Astrophysical Journal Letters*, 437, L43
- Günther, M. N., Zhan, Z., Seager, S., et al. 2019, *arXiv e-prints*, arXiv:1901.00443
- Haffner, L. M., Reynolds, R. J., & Tufte, S. L. 1998, *ApJL*, 501, L83
- Hancock, P. J., Drury, J. A., Bell, M. E., Murphy, T., & Gaensler, B. M. 2016, *Monthly Notices of the Royal Astronomical Society*, 461, 3314
- Hancock, P. J., Hurley-Walker, N., & White T. 2018, *Robbie: Radio transients and variables detection workflow*, *Astrophysics Source Code Library*, , ascl:1808.011
- Hancock, P. J., Murphy, T., Gaensler, B. M., Hopkins, A., & Curran, J. R. 2012, *Monthly Notices of the Royal Astronomical Society*, 422, 1812
- Hancock, P. J., Trott, C. M., & Hurley-Walker, N. 2018, *Publications of the Astronomical Society of Australia*, 35, doi:10.1017/pasa.2018.3
- Hodge, J. A., Becker, R. H., White, R. L., & Richards, G. T. 2013, *The Astrophysical Journal*, 769, 125
- Howell, S. B., Sobek, C., Haas, M., et al. 2014, *PASP*, 126, 398
- Hurley-Walker, N., & Hancock, P. J. 2018, *Astronomy and Computing*, 25, 94
- Hurley-Walker, N., Callingham, J. R., Hancock, P. J., et al. 2017, *MNRAS*, 464, 1146
- Hyman, S. D., Lazio, T. J. W., Kassim, N. E., et al. 2005, *Nature*, 434, 50
- Hyman, S. D., Wijnands, R., Lazio, T. J. W., et al. 2009, *ApJ*, 696, 280
- Intema, H. T., Jagannathan, P., Mooley, K. P., & Frail, D. A. 2017, *Astronomy and Astrophysics*, 598, A78
- Intema, H. T., Jagannathan, P., Mooley, K. P., & Frail, D. A. 2017, *A&A*, 598, A78
- Jaeger, T. R., Hyman, S. D., Kassim, N. E., & Lazio, T. J. W. 2012, *AJ*, 143, 96
- Jones, E., Oliphant, T., Peterson, P., & Others. 2001, *SciPy: Open Source Scientific Tools for Python*, ,
- Lynch, C. R., Lenc, E., Kaplan, D. L., Murphy, T., & Anderson, G. E. 2017, *ApJ*, 836, L30
- Lynch, C. R., Lenc, E., Kaplan, D. L., Murphy, T., & Anderson, G. E. 2017a, *The Astrophysical Journal Letters*, 836, L30
- Lynch, C. R., Murphy, T., Kaplan, D. L., Ireland, M., & Bell, M. E. 2017b, *Monthly Notices of the Royal Astronomical Society*, 467, 3447
- Macquart, J.-P., & Koay, J. Y. 2013, *ApJ*, 776, 125
- Matthews, L. D. 2019, *Publications of the Astronomical Society of the Pacific*, 131, 016001
- McKinney, W. 2010, in *Proceedings of the 9th Python in Science Conference*, ed. S. van der Walt & J. Millman, 51–56
- Metzger, B. D., Williams, P. K. G., & Berger, E. 2015, *ApJ*, 806, 224
- Mooley, K. P., Frail, D. A., Ofek, E. O., et al. 2013, *The Astrophysical Journal*, 768, 165
- Murphy, T., Bell, M. E., Kaplan, D. L., et al. 2015, *MNRAS*, 446, 2560
- Murphy, T., Kaplan, D. L., Croft, S., et al. 2017, *MNRAS*, 466, 1944
- Obenberger, K. S., Taylor, G. B., Hartman, J. M., et al. 2015, *Journal of Astronomical Instrumentation*, 4, 1550004
- Offringa, A. R., de Bruyn, A. G., & Zaroubi, S. 2012, *MNRAS*, 422, 563
- Polisensky, E., Lane, W. M., Hyman, S. D., et al. 2016, *ApJ*, 832, 60

- Ricker, G. R., Winn, J. N., Vanderspek, R., et al. 2015, *Journal of Astronomical Telescopes, Instruments, and Systems*, 1, 014003
- Rowlinson, A., Bell, M. E., Murphy, T., et al. 2016, *MNRAS*, 458, 3506
- Sault, R. J., Teuben, P. J., & Wright, M. C. H. 1995, in *Astronomical Society of the Pacific Conference Series*, Vol. 77, *Astronomical Data Analysis Software and Systems IV*, ed. R. A. Shaw, H. E. Payne, & J. J. E. Hayes, 433
- Sirothia, S. K., Lecavelier des Etangs, A., Gopal-Krishna, Kantharia, N. G., & Ishwar-Chandra, C. H. 2014, *Astronomy and Astrophysics*, 562, A108
- Smith, K. L., Mushotzky, R., Boyd, P. T., et al. 2017, in *American Astronomical Society Meeting Abstracts*, Vol. 229, *American Astronomical Society Meeting Abstracts #229*, 203.02
- Swarup, G. 1991, in *Astronomical Society of the Pacific Conference Series*, Vol. 19, *IAU Colloq. 131: Radio Interferometry. Theory, Techniques, and Applications*, ed. T. J. Cornwell & R. A. Perley, 376–380
- Taylor, M. 2005, in *Astronomical Society of the Pacific Conference Series*, Vol. 347, *Astronomical Data Analysis Software and Systems XIV*, ed. P. Shopbell, M. Britton, & R. Ebert, 29
- The Astropy Collaboration, Robitaille, T. P., Tollerud, E. J., et al. 2013, *Astronomy & Astrophysics*, 558, 9
- Thyagarajan, N., Helfand, D. J., White, R. L., & Becker, R. H. 2011, *The Astrophysical Journal*, 742, 49
- Tingay, S. J., Hancock, P. J., Wayth, R. B., et al. 2016, *AJ*, 152, 82
- Tingay, S. J., Goeke, R., Bowman, J. D., et al. 2013, *PASA*, 30, e007
- Tingay, S. J., Trott, C. M., Wayth, R. B., et al. 2015, *AJ*, 150, 199
- van der Walt, S., Colbert, S. C., & Varoquaux, G. 2011, *Computing in Science & Engineering*, 13, 22
- Villadsen, J., Wofford, A., Quintana, E., Barclay, T., & Thackeray, B. 2018, in *American Astronomical Society Meeting Abstracts*, Vol. 231, *American Astronomical Society Meeting Abstracts #231*, 334.07
- Wehrle, A., Carini, M., & Wiita, P. J. 2018, in *American Astronomical Society Meeting Abstracts*, Vol. 231, *American Astronomical Society Meeting Abstracts #231*, 250.21